Synthesis, Tensile Testing, and Microstructural Characterization of Nanometric SiC Particulate-Reinforced Al 7075 Matrix Composites

A. AHMED, A.J. NEELY, K. SHANKAR, P. NOLAN, S. MORICCA, and T. EDDOWES

This article examines the reasons for the poor performance of the nanometric scale SiC (n-SiC$_p$) particulate-reinforced Al 7075 composites. The composites having different volume fractions of the n-SiC$_p$ were synthesized *via* powder metallurgy (P/M) route and were uniaxially tested at room temperature. Experimental results showed a significant drop in the hardness and tensile properties of the composites in comparison with those of the monolithic Al. Microstructural analysis *via* scanning electron microscopy (SEM) revealed large segregation of Mg in the vicinity of the n-SiC$_p$ and at the grain boundaries of the Al matrix, which plausibly changed both the aging kinetics and tensile behavior of the Al matrix. The segregation of Mg increased with an increase in the volume fraction of the n-SiC$_p$ in the Al matrix. No Mg segregation was found in the monolithic Al. The clustering of the n-SiC$_p$ was observed from SEM with energy dispersive X-ray analysis. SEM also revealed cracks in the n-SiC$_p$ clusters and debonding between the clusters and Al matrix, which were considered as the main mode of fracture in the composites.

DOI: 10.1007/s11661-010-0201-y

I. INTRODUCTION

PARTICULATE (discontinuously) reinforced aluminum matrix composites (AMCs) are emerging as potential advanced composites to replace the monolithic Al alloys for many aerospace, automotive, and structural applications. This is due to their higher stiffness, superior strength to weight ratio, better wear resistance, increased creep resistance, and producibility using the conventional manufacturing processes (casting, powder metallurgy (P/M), *etc*).[1–4] Among Al alloys, Al 7xxx series alloys have the highest strength to weight ratio, which makes them more attractive to be reinforced by a second phase, *i.e.*, ceramic (oxide, nitride, carbide) particulates to eventually form a higher performance composite. Previous investigations, as given in Table I, have so far reported mixed results with both increases and decreases in the strength of the Al 7xxx series alloys reinforced with either micrometric or nanometric scale ceramic particulates.[5–16] Reduced strength has been linked with a number of factors, including the embrittlement effect of the particulate, particulate size, particulate clustering, deceleration in the aging kinetics of the matrix, interfacial reaction between the reinforcement and matrix, porosity issue, and the nature of synthesis route adopted.[10,11,15,16] Some investigations have found[8,9] that nanometric scale reinforcements are better than micrometric scale ones because of their effectiveness in blocking the dislocation motions, and because of their small size, they are less prone to crack or damage during the composite's synthesis process. The challenge while dealing with nanometric scale reinforcements is their natural tendency to cluster due to strong Vander Waals forces because of their tiny geometries, and therefore, they are hard to homogeneously disperse in the metal matrix as compared to micrometric scale reinforcements. This issue can be reduced by keeping the particulate and matrix particle size ratio of nearly 1.[17] However, then there is likely a possibility of a particulate (reinforcement) and matrix reaction at their interface, especially in the case of Al, which is highly chemically reactive in nature. The degree of clustering can be assessed by measuring the coefficient of variance of the mean near-neighbor distance (COV$_d$), which is principally sensitive and effective in characterizing particulate agglomeration.[17] This approach seems to be difficult to apply on nanometric scale particulates, because they cannot be easily resolved even *via* an electron microscope and, hence, it is hard to measure the nearest-neighbor distance of the particles.

Powder metallurgy is one of the most effective techniques to produce this class of composites, because all considerations of solid-liquid phase changes can be ignored, which makes it more flexible than casting, forging, and extrusion forming techniques. The P/M route also has the advantage of reducing the reinforcement and matrix interaction *via* semisolid and solid-state processing.[18] Therefore, the objective of undertaking this work was to produce the n-SiC$_p$/Al 7075 composites using the P/M route and determining the effects of different volume fractions of the n-SiC$_p$, their distribution and

A. AHMED, Ph.D. Student, A.J. NEELY and K. SHANKAR, Senior Lecturers, and P. NOLAN, Technical Staff Member, are with the School of Engineering and Information Technology, University of New South Wales @ Australian Defence Force Academy, Canberra 2600, Australia. Contact e-mail: adnan.ahmed@student.adfa.edu.au S. MORICCA and T. EDDOWES, Staff Members, are with the Materials and Engineering Science Division, ANSTO, Lucas Heights, NSW 2234, Australia.

Manuscript submitted May 23, 2009.
Article published online March 19, 2010

Table I. Comparison of Tensile Properties of Particulate-Reinforced Al 7xxx Composites

Materials	Particle Size (μm)	Volume Fraction (Pct)	E (GPa)	YS (MPa)	UTS (MPa)	Elongation (Pct)	Increase YS (Pct)	Increase TS (Pct)	Temp. (°C)	Ref.
Al7075	—	—	—	552*	619	24**	—	—	RT	5
Al7075/SiC	5	15	—	570*	630	10**	3.2	1.7	RT	
Al7075/SiC	13	15	—	595*	645	4.8**	7.7	1.2	RT	
Al7075/SiC	60	15	—	501*	504	1**	–9.2	–18.5	RT	
Al7075	—	—	—	505	590	15	—	—	RT	6
Al7075/SiC-T6	14	15	—	478	543	7	–5.3	–7.9	RT	
Al7075	—	—	—	174	185	30	—	—	250	
Al7075/SiC-T6	14	15	—	192	202	17	10.3	9.1	250	
Al7075	—	—	—	33	37	104	—	—	400	
Al7075/SiC-T6	14	15	—	33	37	46	0	0	400	
Al7075	—	—	66.4	577*	603	11.8	—	—	RT	10
Al7075/SiC	50 nm	1	62.9	471*	505	9.8	–18.3	–16.2	RT	
Al7075/SiC	50 nm	5	72	485*	514.3	6.1	–15.9	–14.7	RT	
Al7075	—	—	57.1	260.5*	262.2	50.4	—	—	215	
Al7075/SiC	50 nm	1	55.2	237*	239.5	33.6	–9	–8.6	215	
Al7075/SiC	50 nm	5	58	244*	245	19.5	–6.3	–6.5	215	
Al7075	—	—	39.2	43.5*	44.4	86.8	—	—	350	
Al7075/SiC	50 nm	1	43.2	44.5*	47	74	2.5	5.8	350	
Al7075/SiC	50 nm	5	33.2	43.6*	44.3	38	0.2	–0.2	350	
Al7091-T6	—	—	68.5	520	590	10.2	—	—	RT	11
Al7091/SiC-T6	5	15	90.7	480	530	3.1	–7.7	–10.1	RT	
Al7091/SiC-T6	16	15	99.1	490	535	1.1	–5.7	–9.3	RT	
Al7091/SiC-T6	5	20	94.1	400	470	1.9	–23	–20.3	RT	
Al7091/SiC-T6	16	20	101.4	500	560	1.8	–3.8	–5	RT	
Al7093-T6	—	—	67.5	566	622	10	—	—	RT	7
Al7093/SiC-T6	10	15	95.6	642	694	1.8	13.4	11.5	RT	
Al7775-T6	—	—	—	534*	592	13	—	—	RT	8
Al7775/SiC-T6	13	10	—	507*	566	7	–5	–4.4	RT	
Al7775/SiC-T6	50 nm	1	—	583*	635	7	9.1	7.2	RT	
Al7775/SiC-T6	50 nm	5	—	552*	594	3	3.3	0.3	RT	
Al7775/Al_2O_3-T6	50 nm	1	—	551*	602	5	3.2	1.7	RT	
Al7775/Al_2O_3-T6	50 nm	5	—	313*	375	4	–41.3	–36.6	RT	
Al7075-T6	—	—	—	533*	574	9.6	—	—	RT	9
Al7075/SiC-T6	50 nm	1	—	599*	634	8.9	12.4	10.4	RT	
Al7075/SiC-T6	50 nm	5	—	527*	547	3.1	–1.1	–4.7	RT	

*0.2 pct yield stress.
**Percent reduction in area.

clustering on the grain structure, aging kinetics, tensile properties, and fracture mechanics of the composites.

II. EXPERIMENTAL PROCEDURE

A. *Synthesis*

High-strength aluminum Al 7075 (composition Al-Zn5.4-Mg2.9-Cu1.6-Cr0.29 wt pct) with a particle size of 36 to 71 μm and nodular shape was used as the matrix (source: ECKA Granules, Velden GmbH, Germany), as shown in Figure 1(a). The nanometric SiC particulates (n-SiC_p) with a mean size of 50 nm and polygonal shape were used as the reinforcement (source: National Taiwan University, Taipei, Taiwan, ROC), as shown in Figure 1(b). The P/M route used consisted of wet mixing of the powders, cold isostatic pressing (CIP), degassing, sintering, and hot isostatic pressing (HIP). A high energy attritor (ball mill), having a ceramic walled vial filled with 5-mm-diameter zirconia balls, was used to blend the powders to produce a homogeneous mixture. Attrition milling was preferred because the milling intensity of an attritor is much higher, at least one order of magnitude difference in time to achieve similar results.[18] The Al was blended with different volume fractions (1 and 5 vol pct) of the n-SiC_p in an ethanol slurry in a water-cooled attritor rotating at 250 rpm. A balls-to-material weight ratio of 10:1 was used. Ethanol was used to reduce oxidation of the Al and to act as a neutral medium for the uniform dispersion of the n-SiC_p. Milling was performed for 15 minutes for the purpose of mixing the powders. The mixtures were then dried followed by CIP at 400 MPa for 5 minutes to form green bodies (having density of 75 pct of the theoretical density). Those were then degassed and sintered in a nitrogen atmosphere at 590 °C for 3 hours. HIP was performed at 520 °C and 100 MPa for 3 hours in argon atmosphere in an attempt to further increase the density of the samples. Finally, the hot isostatically pressed (''hipped'') compacts were hot extruded at 480 °C with

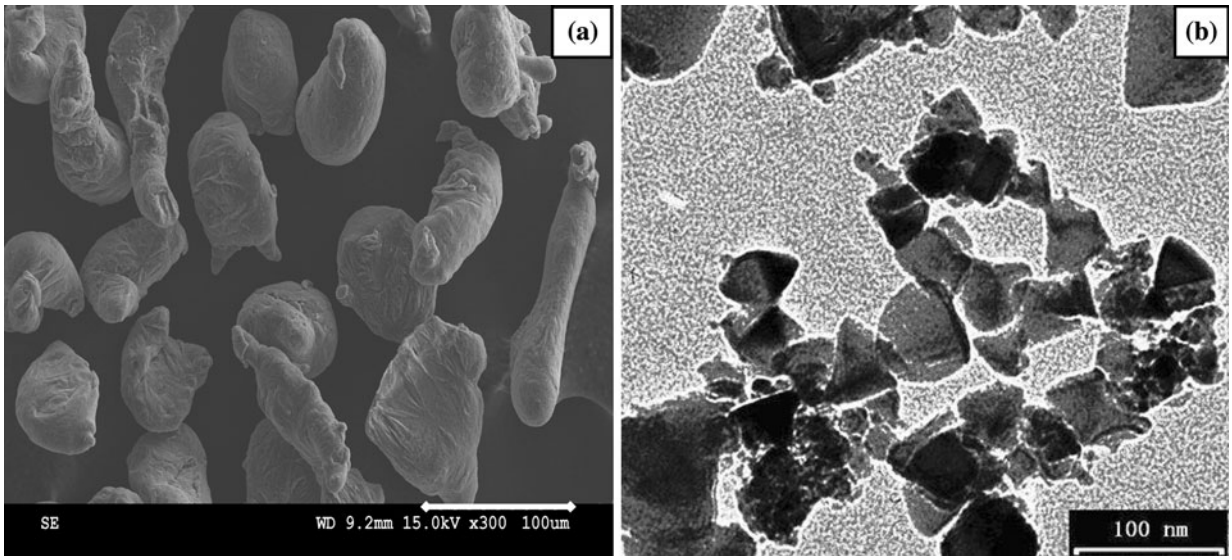

Fig. 1—(*a*) SEM micrograph of as-received Al 7075 powder and (*b*) TEM micrograph of ultrasonically dispersed *n*-SiC_p.

Table II. Densities of Monolithic Al and *n*-SiC_p/Al Composites during Different Synthesis Phases

Material	Density (before HIP) (kg/m^3)	Density (As-Hipped) (kg/m^3)	Density (As-Extruded) (kg/m^3)	Theoretical Density (kg/m^3)
Al 7075	2785	2790	2794	2800
1 vol pct *n*-SiC_p/Al	—	2562	2823	2803
5 vol pct *n*-SiC_p/Al	—	2496	2807	2815

an area reduction ratio of 12:1, to form fully dense cylindrical rods of 8-mm diameter. The densities of the samples were measured using the Archimedes principle, as given in Table II. Before the tensile testing, all the rods were T6 heat treated (peak aged) and machined to dog-bone-shape specimens having a gage length of 25 mm and a circular cross section of 4-mm diameter.

B. *Mechanical Testing*

Uniaxial tensile tests were performed at room temperature using an Instron servohydraulic material testing machine at a crosshead speed of 1 mm/min. Three samples were tested for each composition of the material. A laser extensometer was used to measure deformation until the failure point in the test samples. Engineering stress-strain curves were plotted to measure the elastic modulus (E), 0.2 pct yield strength (YS), ultimate tensile strength (UTS), and ductility of the samples.

C. *Microstructural Analysis*

For grain structure analysis, all the samples were ground and polished down to 1 μm using diamond suspension sprays and were etched using aqueous orthophosphoric acid (0 to 10 pct) before being examined under an optical microscope (OM). The aging kinetics of the samples were studied by first solution treating them at 480 °C for 2 hours followed by water quenching. Subsequently, all the samples were aged at 120 °C, for different intervals of time from 0 to 100 hours, in an oil bath to ensure they all aged at constant temperature, and after that, they were water quenched. Before the hardness testing, all the samples were ground and polished down to 1 μm using diamond suspension sprays. Rockwell hardness tests were performed to study the age hardening in the samples. A load of 100 kg was applied for 5 seconds using a steel ball 1/16-in. (1.587-mm) diameter indenter, and 10 indentations were measured on each sample.

Scanning electron microscopy (SEM) with the energy dispersive X-ray analysis feature was used to determine clustering of the *n*-SiC_p, composition of various regions in the samples, especially of the *n*-SiC_p-matrix interface, and to do fractography on the fracture surfaces of the tested samples to investigate the nature of failure in the materials. ImageJ (version 1.37, http://rsbweb.nih.gov/ij/) software was used to measure the grain sizes and the degree of clustering of the *n*-SiC_p, from the OM micrographs of the samples.

III. RESULTS

A. *Grain Structure*

OM micrographs of the transverse sections of the monolithic Al and the 5 vol pct *n*-SiC_p reinforced Al composites are shown in Figure 2. The grain sizes of the monolithic Al, the 1 vol pct, and the 5 vol pct *n*-SiC_p

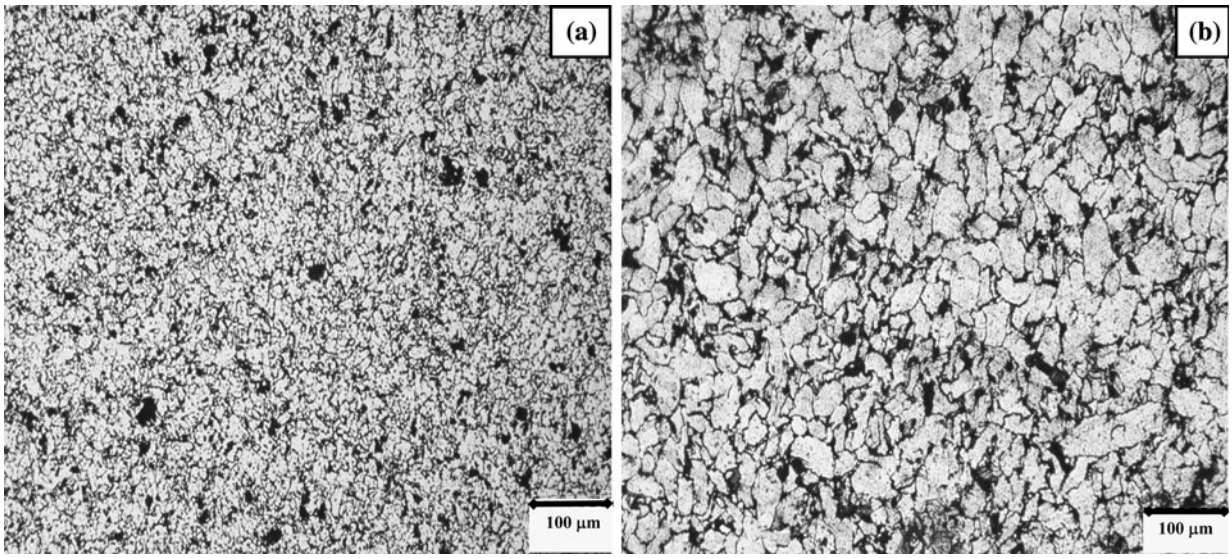

Fig. 2—Grain structures of (*a*) monolithic Al and (*b*) 5 vol pct *n*-SiC_p/Al composite, after etching.

reinforced Al composites were measured to be 11.2, 20, and 25.3 μm, respectively. It is apparent qualitatively that, unlike other studies,[8,9] incorporation of *n*-SiC_p did not refine the grain size of the composites. In fact, the grain structure of the composites was found to be coarser than the monolithic Al, as shown in Figure 2. Kang[8] reported that *n*-SiC_p could refine the grain size by pinning the grain boundaries of the Al matrix, which might add a little to the strength of the matrix. The reason for the difference in the grain sizes of the unreinforced Al and the composites are discussed in the Section IV–B.

B. *Aging Kinetics*

The Rockwell B hardness (HRB) aging curves of the monolithic Al and the *n*-SiC_p reinforced Al composites are given in Figure 3. Within 40 hours, all the samples were peak aged (achieved maximum hardness) at an aging temperature of 120 °C, as shown in Figure 3. After artificial aging, monolithic Al achieved the hardness that agreed with the published data. Exceptionally less precipitation hardening was noticeable in the composites. A drop of 30 to 35 pct was measured in the hardness of the composites in comparison with that of the monolithic Al. This large drop in the hardness values of the composites was due to the unavailability of the Mg atoms in the microstructure of the Al matrix, which substantially reduced the precipitation of strengthening phase such as $MgZn_2$. In the as-extruded condition, the hardness of both the monolithic Al and the composites was found to be similar. From the aging curve, as shown in Figure 3, it was plausible that Mg segregation occurred during the solution treatment and water quenching of the composites, because the drop in the hardness of the composites was still apparent and significant at the start of artificial aging at 120 °C. After artificial aging, there was less improvement in the hardness of the composites as compared to that of the monolithic Al. The plausible causes of Mg segregation are discussed in detail in Section IV–B.

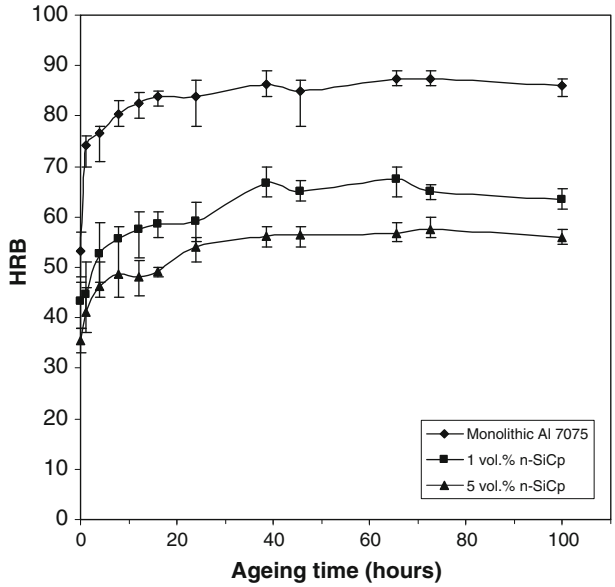

Fig. 3—HRB aging curves of monolithic Al and *n*-SiC_p/Al composites solution heat treated and artificially aged.

C. *Tensile Properties*

A significant reduction was observed in the tensile properties of the composites, as shown in Figure 4. Stiffness-wise, the monolithic and the *n*-SiC_p reinforced Al composites were found to be similar. However, the addition of just 1 vol pct of *n*-SiC_p drastically reduced the strength and ductility of the composites. This trend continued with an increase in the volume fraction of *n*-SiC_p. The substantial drop in the strength of the composites was found to be caused by the reduced artificial aging of the composites, which was linked to

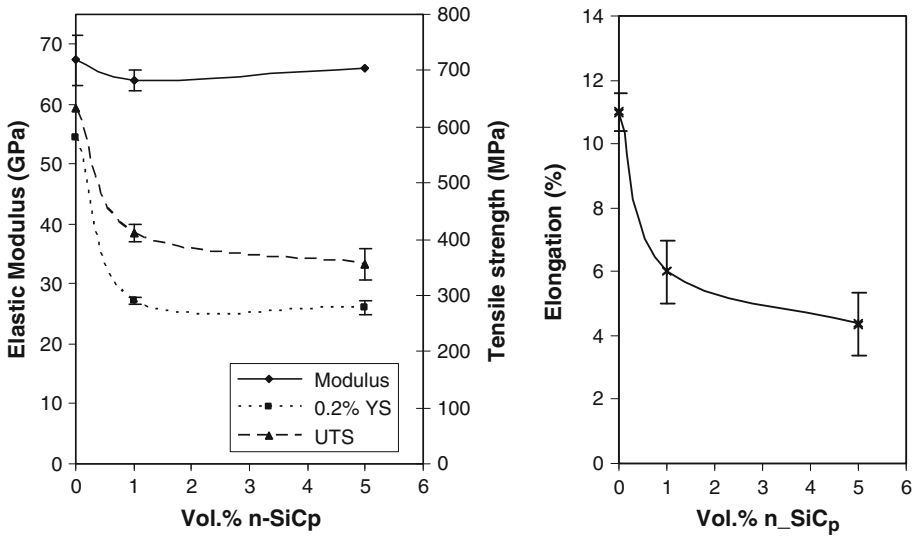

Fig. 4—Elastic modulus, 0.2 pct YS, UTS, and ductility of monolithic Al and *n*-SiC_p/Al composites at room temperature.

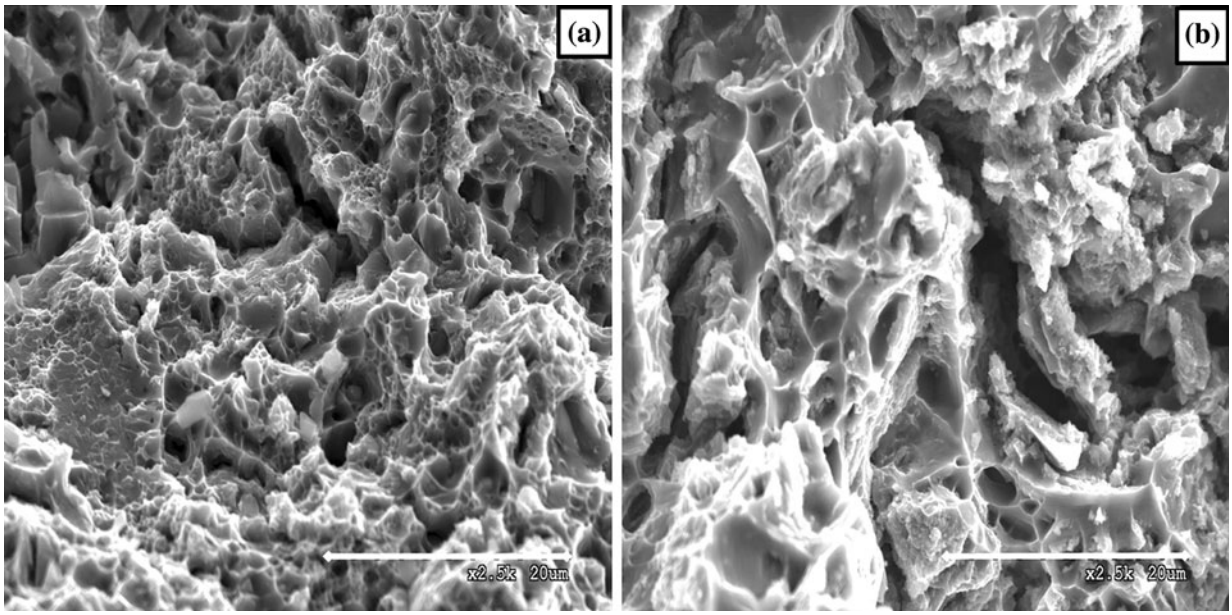

Fig. 5—Fractographs of fracture surfaces of (*a*) monolithic Al and (*b*) 5 vol pct *n*-SiC_p/Al composite tested in tension.

the reactivity of Mg with O and its segregation at the grain boundaries and the SiC-Al interface, as explained in Section IV–B.

D. *Fractography*

Fractography was used to examine the failure mechanisms of the materials. At macroscopic scale, ductile fracture was observed in the monolithic Al. Fracture was brittle in appearance in the composites as the fracture surfaces were flat and less plastic deformations were apparent in the tensile tests data. SEM revealed that the deformation was not fully brittle in the composites; in fact, it was a combination of both the ductile and brittle modes, as shown in Figure 5. Shallow dimples and intergranular fractures were seen in all the fractographs. Fracture was initiated by the formation of microvoids, following their nucleation and coalescence. The microvoids on the ruptured surfaces of the composites were found to contain large amounts of *n*-SiC_p and its clusters, as shown in Figure 6, signifying that they provided sites for the rupture of the composites, which accelerated the damage in the composites.

IV. DISCUSSION

A. *Aggregation of n-SiC_p*

SEM revealed that the *n*-SiC_p was not homogeneously distributed in the Al matrix and clustered mainly at the

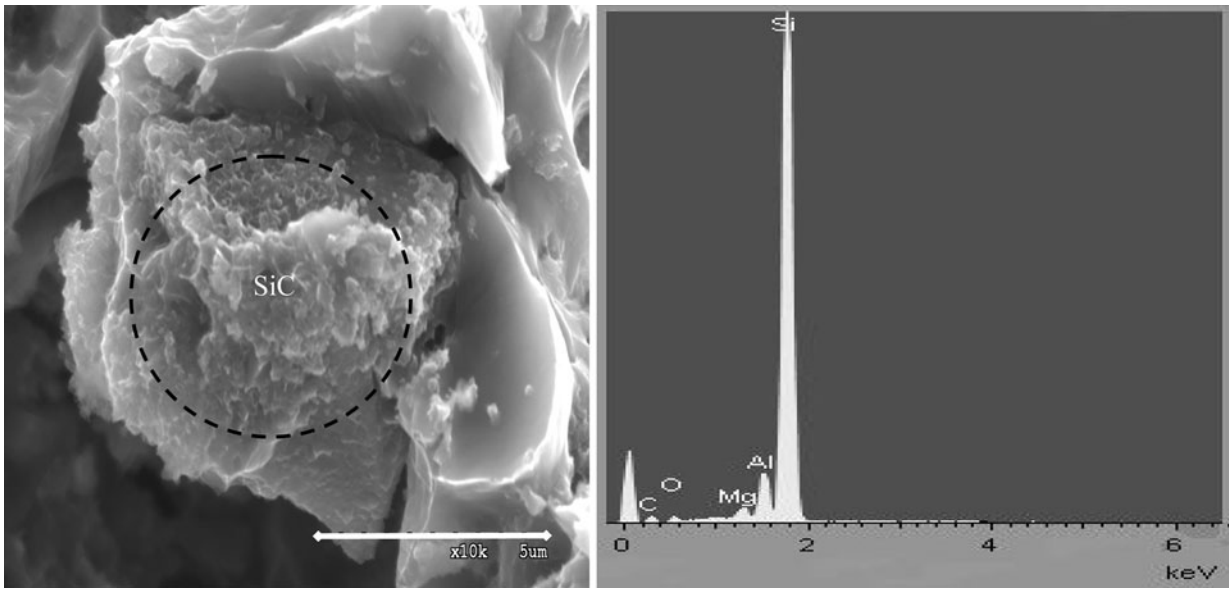

Fig. 6—Fractograph with X-ray spectrum showing a cluster of n-SiC$_p$ at a microvoid in 5 vol pct n-SiC$_p$/Al composite.

grain boundaries, as shown in Figure 7. This was possibly due to the large difference in size between the Al and the SiC particles, which pushed the n-SiC$_p$ into the gaps between the Al particles. Wet mixing of the powders did not facilitate the uniform dispersion of n-SiC$_p$, and it unexpectedly aggravated the agglomeration of the particles. Clustering of the n-SiC$_p$ can be catastrophic for the composite; since SiC$_p$ and its clusters are stiffer than the matrix, they can bear more load by restricting plastic deformation and, hence, act as stress concentrators. Therefore, clusters are more prone to crack and/or interface failure,[19] particularly in the matrix with reduced precipitates.

B. *Segregation of Mg*

The aging kinetics and tensile behavior of the composites were significantly altered by the addition of n-SiC$_p$. Monolithic Al 7075 synthesized using the same P/M route exhibited properties that agreed with published data and in which no segregation of Mg was found. This suggests that the adopted manufacturing route was appropriate for the monolithic Al, though it did not guarantee the same for the composites. The low mechanical performance of the n-SiC$_p$/Al composites, therefore, is possibly linked with the reactions that occurred at the n-SiC$_p$-Al interfaces and at the grain boundaries, which adversely changed the microstructure and tensile properties of the Al matrix.

The SEM with X-ray mapping feature depicted enormous segregation of the highly reactive Mg at the n-SiC$_p$-Al interfaces and at the grain boundaries of the composites-T6, as shown in Figure 8. The segregation of Mg in the Al-Mg matrix composites has been widely studied.[8,20–24] Mg can segregate at the grain boundaries, free surfaces, and interfaces of the Al matrix. There are two major types of segregations: equilibrium segregation and nonequilibrium segregation. Equilibrium segregation is the enrichment of dilute solute elements (alloying elements) at the dislocations, grain boundaries, free surfaces, or interfaces within the solids.[25] This segregation is thermodynamically governed to minimize the grain boundary energy, interface energy, or free surface energy of the system.[26] Nonequilibrium segregation arises as a result of solutes being dragged or pulled to point defects or vacancies, which move to grain boundaries or sinks during quenching (heat treatment). It can also occur as a result of solute pileup at a moving interface.[27] In composites, the reinforcement-matrix interface acts like a good sink for the solute atoms during the heat treatment and cooling processes.[24] Perhaps, nonequilibrium segregation can be minimized and possibly avoided by maintaining a low solution treatment temperature and fast cooling rate.[28]

Now, the question arises that, among Zn, Mg, and Cu, which were the major alloying elements in Al 7075, why only Mg enriched the reinforcement-matrix interfaces and the grain boundaries? One reason could be the atomic weight of the Mg atom. In the periodic table, Mg is the lightest element among $_{30}Zn^{65.38}$, $_{29}Cu^{63.54}$, and $_{12}Mg^{24.3}$. Consequently, it would be relatively easier for Mg to flow and fill the vacancies created at the grain boundaries and interfaces due to nonequilibrium segregation. Second, Mg is naturally a highly reactive element. It was reported that the tendency of Mg to form oxide is about 10^8 times higher than that of Al at any temperature.[29] In our adopted synthesis route, the wet slurry of the n-SiC$_p$ and Al 7075 powders was dried in air at 45 °C, which took 8 to 10 days to achieve a dried mixture free of ethanol. In the case of Al powder, a very thin oxide layer is always formed on the surface of the particles. During the extremely slow drying phase, oxidation of the n-SiC$_p$ mixed with Al was possible. The X-ray maps confirmed a high level of oxygen linked to Mg at the interfaces and the grain boundaries, as shown in Figure 8. The source of oxygen could be the oxidized

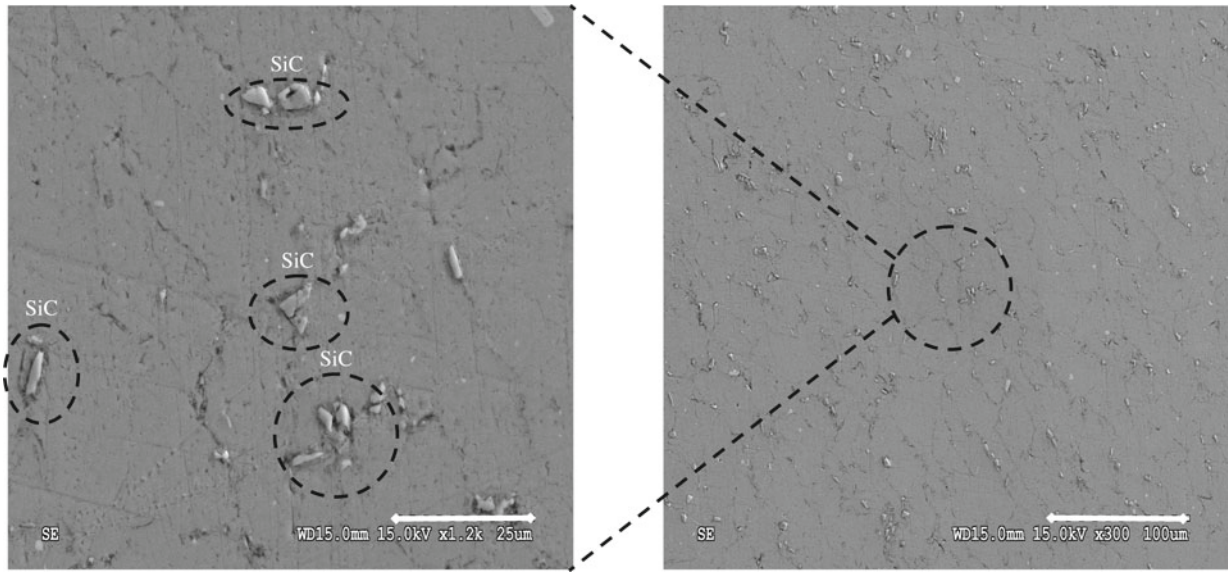

(a)

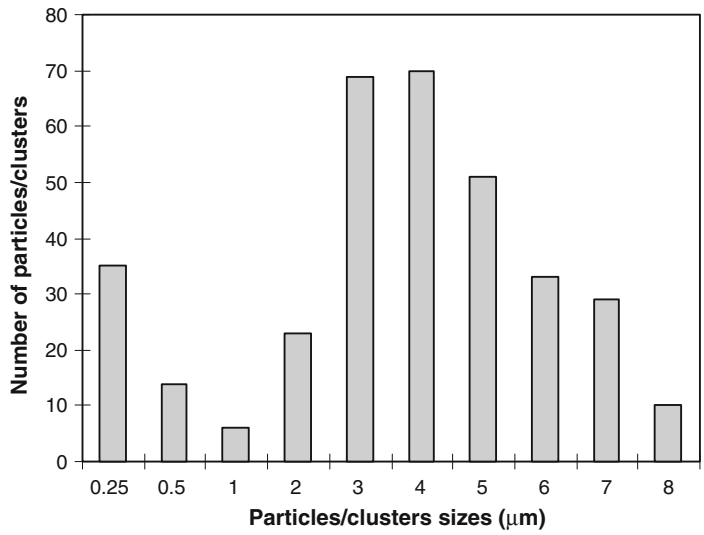

(b)

Fig. 7—(*a*) SEM micrographs showing clusters of *n*-SiC_p sitting at grain boundaries with corresponding (*b*) degree of clustering in 5 vol pct *n*-SiC_p/Al composite.

Al, *i.e.*, Al_2O_3 or oxidized SiC with a very thin layer of SiO_2. Subsequently, all the samples went through intensive heat treatment cycles. Initially, all samples were sintered for 3 hours at 595 °C followed by HIP at 520 °C and 100 MPa for 3 hours. Finally, they were T6 heat treated. These extreme heat cycles, especially HIP, may have been enough to induce Mg to react with the oxidized *n*-SiC_p-Al interfaces and the grain boundaries. The following reactions[23] could occur in this case:

$$Mg + O_2 = MgO \quad [1]$$

$$2Mg + SiO_2 = MgO + Si \quad [2]$$

$$4Al + SiO_2 = Al_2O_3 + Si \quad [3]$$

$$Mg + 2Al + 2SiO_2 = MgAl_2O_4 + 2Si \quad [4]$$

$$2MgO + 4Al + 3SiO_2 = 2\,MgAl_2O_4 + 3Si \quad [5]$$

$$MgO + Al_2O_3 = MgAl_2O_4 \quad [6]$$

$$3Mg + 4Al_2O_3 = 3MgAl_2O_4 + 2Al \quad [7]$$

In the as-extruded materials, similar hardness values were found for both the monolithic Al and the composites. From the aging curve, as shown in Figure 3, it was plausible that Mg segregation occurred during the solution treatment of the composites, because the drop in the hardness of the composites was still apparent and

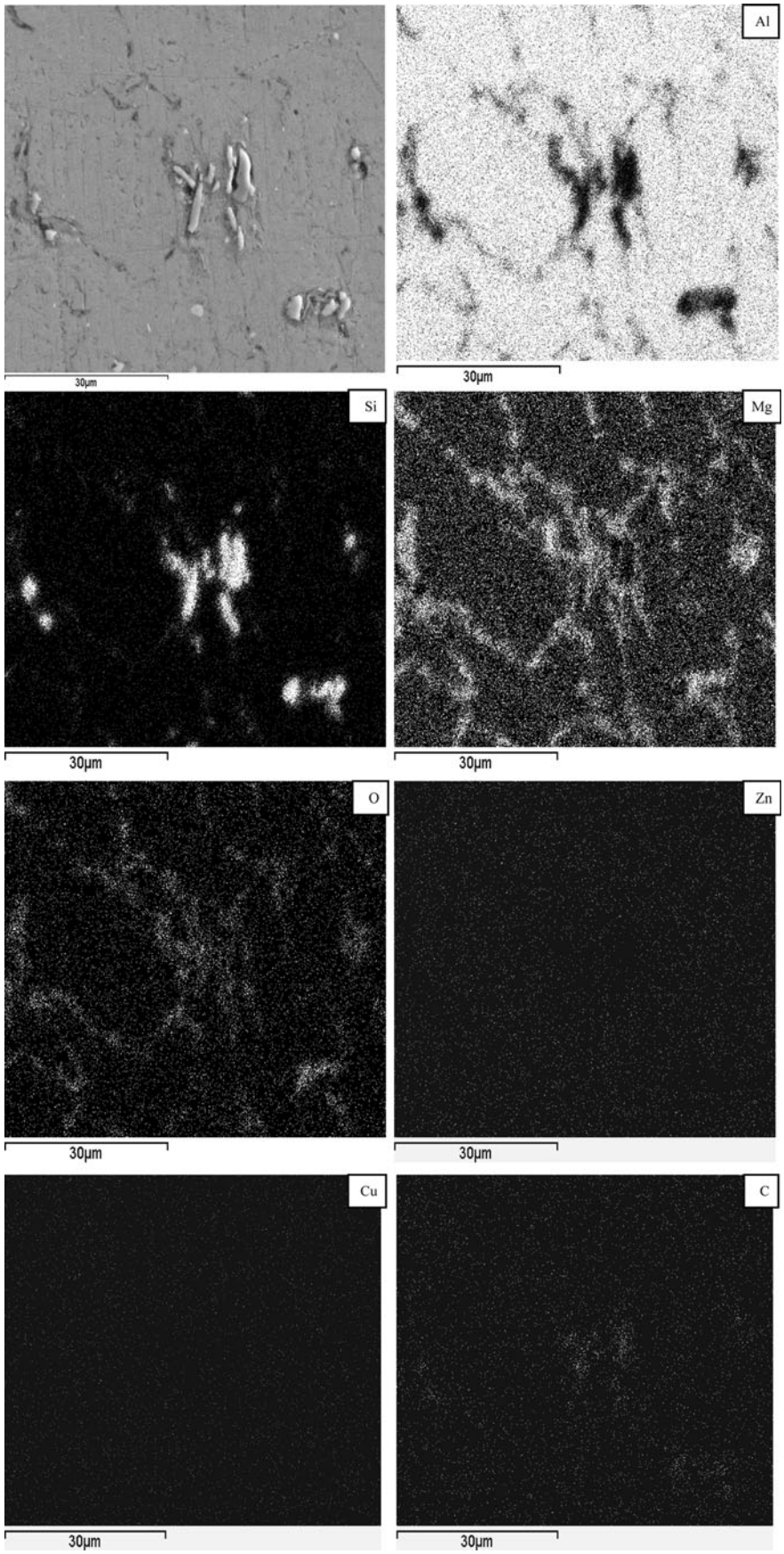

Fig. 8—SEM micrograph with X-ray maps showing distribution of alloying elements, *n*-SiC_p, and oxygen content in 5 vol pct *n*-SiC_p/Al composite.

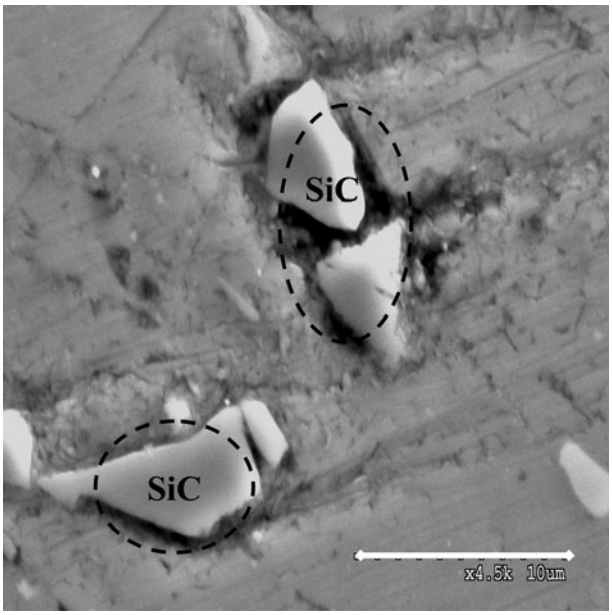

Fig. 9—SEM micrographs illustrating microvoids, Al-SiC interface failure, and cracking of n-SiC_p clusters.

significant at the start of the artificial aging at 120 °C. After artificial aging, there was less notable improvement in the hardness of the composites as compared to that of the monolithic Al. No segregation was observed in the monolithic Al, because it did not pass through the wet mixing and drying process in the atmospheric conditions. It did not contain the n-SiC_p, which can act as a sink for the Mg to be deposited at the Al-SiC interface, and also, there was no likelihood for an interfacial reaction, which is likely to occur at a high temperature at the Al-SiC interface and could be detrimental to the composite's properties.

It is conceivable that the segregation of Mg was largely caused by the interfacial reaction of Mg with the oxidized n-SiC_p-Al layers and the grain boundaries. During age hardening, this reaction drastically reduced the precipitation of the major strengthening phase ($MgZn_2$)[8,9] due to lack of Mg atoms in the Al matrix, which ultimately resulted in the reduced hardness and strength of the composite.

Coarser grain size of the composites could also be associated with less precipitation effect, which did not refine the microstructure. Precipitates are normally tens of nanometers in size and are very effective in pinning the dislocations. They also pin the grain boundaries and refine the grain structure of the material. Thus, it can be concluded that, in this particular case, Mg segregation was the core cause of the low hardness and tensile strength of the composites.

C. *Mode of Fracture*

Fracture in particulate-reinforced composites is strongly dependent on the particulate strength and particulate-matrix interface strength. Fracture can occur in the form of particulate fracture, near particulate fracture, debonding between matrix and reinforcement, near interface failure, and fracture between particulate agglomerations.[30–33] Particulate fracture or a weak interface is unlikely in nanometric scale particulate-reinforced composites, because the particles are less likely to contain defects or to be damaged during the material's synthesis process.[8] However, they are more prone to particulate clustering,[34] which could severely degrade the strength and ductility of the matrix by initiating localized damage. In the present study, the composites failed before reaching the yield strength of the Al matrix. It was observed *via* SEM, as shown in Figure 9, that the damage began first at the n-SiC_p clusters in the composites. Because there was less precipitation hardening effect in the composites, the applied load was mostly concentrated at the n-SiC_p clusters. So, microvoids may have first emerged at or in the vicinity of these clusters, which nucleated, grew, and coalesced, and then the final rupture occurred through the matrix between the debonded or broken clusters.[35]

V. CONCLUSIONS

By the addition of n-SiC_p, a drastic variation was found in the microstructure and tensile properties of the Al 7075 alloy. No grain refinement was observed in the composites. The grain structure of the composites was found to be coarser than that of the monolithic Al. The hardness and tensile strength of the composites were found to be fairly low (25 to 35 pct and 35 to 44 pct drop in the hardness and ultimate tensile strength of the composites, respectively) in comparison with that of the monolithic Al synthesized using the same P/M route. This discrepancy in the tensile properties increased with an increase in the volume fraction of the n-SiC_p. Deterioration in the properties is believed to be linked to the segregation of Mg at the oxidized n-SiC_p-Al interfaces and grain boundaries, which resulted in reduced precipitation hardening of the Al matrix. Clustering of n-SiC_p was observed and it was speculated that the fracture in the composites was governed by the debonding and cracking of the n-SiC_p clusters.

ACKNOWLEDGMENTS

The authors are grateful to the University of New South Wales @ Australian Defence Force Academy for supporting the research work reported in this article. The authors are obliged to the Australian Institute of Nuclear Science and Engineering (AINSE) for supporting the materials' synthesis performed at the Australian Nuclear Science and Technology Organization (ANSTO) under AINSE Grant No. AINGRA07167. The authors also thank the Electron Microscopy Unit (EMU), Australian National University, Canberra for assisting with the SEM.

REFERENCES

1. D.L. McDanels: *Metall. Trans. A*, 1985, vol. 16A, pp. 1105–15.
2. T.S. Srivatsan: *J. Mater. Sci.*, 1996, vol. 12, pp. 1375–88.
3. M. Taya and R.J. Arsenault: *Metal Matrix Composites Thermomechanical Behaviour*, Pergamon Press, New York, NY, 1989, pp. 2–5.
4. T.W. Clyne and P.J. Withers: *An Introduction to Metal Matrix Composites*, University Press, Cambridge, United Kingdom, 1993, p. 5.
5. T.J.A. Doel and P. Bowen: *Compos. Part A*, 1996, vol. 27, pp. 655–65.
6. A. Razaghian, D. Yu, and T. Chandra: *Compos. Sci. Technol.*, 1998, vol. 58, pp. 293–98.
7. A.B. Pandey, B.S. Majumdar, and D.B. Miracle: *Metall. Mater. Trans. A*, 2000, vol. 31A, pp. 921–36.
8. Y.C. Kang: Ph.D. Thesis, National Taiwan University, Taipei, Taiwan, ROC, 2004, pp. 134–45.
9. Z. Ren: M.E. Thesis, University of New South Wales, Sydney, Australia, 2007, p. 50.
10. A. Ahmed, A.J. Neely, K. Shankar, and S.L.I Chan: *Mater. Sci. Forum*, 2007, vols. 561–565, pp. 761–64.
11. J.K. Shang and R.O. Ritchie: *Acta Metall.*, 1989, vol. 37, pp. 2267–78.
12. A.N. Tiwari, V. Gopinathan, and P. Ramakrishan: *Mater. Manuf. Processes*, 1991, vol. 6, pp. 612–33.
13. A. Kalkanli and S. Yilmaz: *Mater. Des.*, 2008, vol. 29, pp. 775–80.
14. C.H.J. Davies: *J. Mater. Process. Technol.*, 1996, vol. 62, pp. 225–28.
15. L.E.G. Cambronero, E. Sanchez, J.M. Ruiz-Roman, and J.M. Ruiz-Prieto: *J. Mater. Process. Technol.*, 2003, vols. 143–144, pp. 378–83.
16. N.V. Ravi Kumar and E.S. Dwarakadasa: *J. Mater. Sci.*, 1994, vol. 29, pp. 1533–39.
17. N. Chawla and K.K. Chawla: *Metal Matrix Composites*, Springer, New York, NY, 2006, pp. 88–90.
18. F. Thummler and R. Oberacker: *Introduction to Powder Metallurgy*, University Press, Cambridge, United Kingdom, 1993, pp. 10–12.
19. T.S. Srivatsan and V.K. Vasudevan: *Int. J. Fatigue*, 1998, vol. 20, pp. 187–202.
20. X.G. Ning, J. Pan, J.H. Li, K.Y. Hu, H.Q. Ye, and H. Fukunaga: *J. Mater. Sci. Lett.*, 1993, vol. 12, pp. 1644–47.
21. M. Strangwood, C.A. Hippsley, and J.J. Lewandowski: *Scripta Metall. Mater.*, 1990, vol. 24, pp. 1483–87.
22. D.P. Myriounis, S.T. Hasan, and T.E. Matikas: *Compos. Interfaces*, 2008, vol. 15, pp. 495–514.
23. Z. Shi, M. Gu, J. Liu, G. Liu, J.-C. Lee, D. Zhang, and R. Wu: *Chin. Sci. Bull.*, 2001, vol. 46, pp. 1948–52.
24. W.M. Zhong, L'Esperance, and M. Suery: *Metall. Mater. Trans. A,* 1995, vol. 26A, pp. 2637–49.
25. J.H. Westbrook: *Metall. Rev.*, 1964, vol. 9, pp. 415–70.
26. D. McLean: *Grain Boundaries in Metals*, University Press, Oxford, United Kingdom, 1957, p. 118.
27. J.R. Rellick and C.J. McMahon: *Metall. Trans.*, 1974, vol. 5, pp. 2439–50.
28. D.R. Harries and A.D. Marwick: *Phil. Trans. R. Soc. London A*, 1980, vol. 295, pp. 197–207.
29. D.R. Gaskell: *Introduction to Metallurgical Thermodynamics*, Hemisphere, New York, NY, 1981, p. 287.
30. R. Arone, O. Botstein, and B. Shpigler: *Isr. J. Technol.*, 1988, vol. 24, pp. 393–99.
31. S.V. Kamat, J.O. Hirth, and R. Mehrabian: *Acta Metall.*, 1989, vol. 37, pp. 2395–2402.
32. Y. Flom and R.J. Arsenault: *Acta Metall.*, 1989, vol. 37, pp. 2413–23.
33. D.J. Lloyd, H. Lagace, A. McLeod, and P.L. Morris: *Mater. Sci. Eng. A*, 1989, vol. 107, pp. 73–80.
34. T.J.A. Doel and P. Bowen: *Compos. Part A*, 1996, vol. 27, pp. 655–65.
35. D.J. Lloyd: *Acta Metall. Mater.*, 1991, vol. 39, pp. 59–71.